

Sandwich Complexes | Hot Paper |

Electron- and Hydride-Reservoir Organometallics as Precursors of Catalytically Efficient Transition Metal Nanoparticles in Water

Fangyu Fu,^[a] Qi Wang,^[a] Roberto Ciganda,^[a, b] Angel M. Martinez-Villacorta,^[c] Ane Escobar,^[c] Sergio Moya,^[c] Eric Fouquet,^[a] Jaime Ruiz,^[a] and Didier Astruc*^[a]

Abstract: Nanoparticles (NPs) are actively investigated for their efficient use in catalysis, but their means of synthesis is a key factor influencing their catalytic properties owing to surface coverage with byproducts. Here, neutral electron- and hydride-rich late transition metal organometallics are compared for the synthesis of late transition metal NPs in the presence of poly(vinylpyrrolidone) (PVP). In particular, the effect of electron-reservoir donors, hydride-reservoir donors, and electron-rich dimers yielding NPs electrostatically stabilized by cationic organometallics are compared in terms of NP size and catalytic efficiency. The catalytic reactions scruti-

nized with excellent results include 4-nitrophenol reduction to 4-aminophenol by NaBH₄ for the AuNPs and PdNPs, and Suzuki–Miyaura reactions for the PdNPs. The nature of the reductant has more influence on the NP size in the case of AuNPs than PdNPs, and the best NP catalysts are obtained with hydride-reservoir complexes as reductants. The less bulky hydride donors are superior, with the complex [CoCp(η⁴-C₅H₆)] (Cp = η⁵-C₅H₅) giving the NPs with the best catalyst efficiencies for both reactions. Protection of the NP cores by the organometallic sandwich salt is found to be the key to catalytic efficiency.

Introduction

Nanoparticles (NPs) have increasingly been shown to be an essential part of academic research in catalysis; their methods of synthesis are crucial for their catalytic efficiency, and are still constantly investigated and optimized.^[1] So far, sodium borohydride has been the most frequently used reductant of precursor metal salts for the synthesis of transition metal nanoparticles (TMNPs),^[2] but organoboranes formed in organic solutions and borates formed in aqueous solution partly inhibit the catalytic activity of the TMNP surface.^[3] Therefore, a number of other reductants have been probed successfully, including H₂, NaBH₄, (SiMe₂)₆, Mg, Li or Na in liquid NH₃, and Li or Na naphthalenide in the presence of a stabilizer.^[1],4]

Here, we use as reductants electron-rich^[5] and hydride-rich neutral organometallics,^[6] for which both the reduced and oxidized forms are stable. Thus, following the reduction of the metal salts, these organometallics are found to be relatively

bulky cationic stabilizers of the TMNPs. This strategy has recently been probed with ferrocenes upon the reduction of HAuCl₄ to form AuNPs with various late transition metal salts.^[7] With ferrocene itself, large AuNPs were formed owing to the weak driving force resulting from the weak reducing power of ferrocene.^[7] Here, the goal is to compare various electron-reservoir systems with very negative redox potentials with hydride donors of closely related structures. The electron-reservoir systems are known 19-electron Fe^I sandwich complexes of the [FeCp(η⁶-arene)] series (Cp = η⁵-cyclopentadienyl).^[5] The parent compound [FeCp(η⁶-C₆H₆)] is not stable at room temperature (RT) and disproportionates in THF to ferrocene and iron metal, and dimerizes slowly in pentane at RT.^[8] Derivatives with methyl groups on the arene ligand are more stable but behave similarly, except the hexamethylbenzene complex [FeCp(η⁶-C₆Me₆)], which is stable up to 100 °C and for which the X-ray crystal structure and very low ionization potential determined by He^I photoelectron spectroscopy are known (inter alia).^[5,9] Here, both the benzene and hexamethylbenzene iron complexes are used, as well as the dimer of the mesitylene complex and the hydride adducts. The three types of neutral iron sandwich compounds, 19-electron complex, dimer, and hydride derivative, all give the cationic structure upon reduction of a substrate such as the TM precursor salt, as shown in Scheme 1.

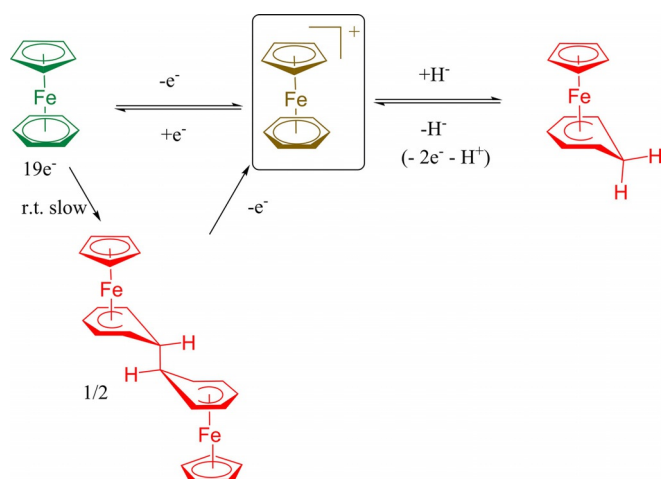
These Fe complexes are compared to ferrocene (FeCp₂) and cobaltocene (CoCp₂)^[10] and its hydride derivative [CoCp(η⁴-C₅H₅)], which also give the same cobalticinium salt upon substrate reduction (Scheme 2).^[11] Decamethylferrocene is avoided because it combines both disadvantages of a poor reductant (given its weak driving force) and bulky donor (providing long-

[a] Dr. F. Fu, Dr. Q. Wang, Dr. R. Ciganda, Prof. E. Fouquet, Dr. J. Ruiz, Prof. D. Astruc
ISM, UMR CNRS N° 5255, University of Bordeaux
33405 Talence Cedex (France)
E-mail: didier.astruc@u-bordeaux.fr

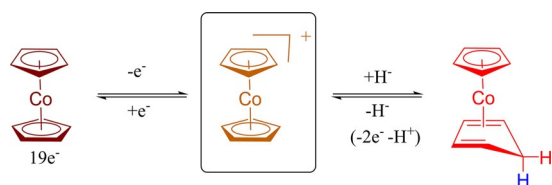
[b] Dr. R. Ciganda
Facultad de Quimica, Universidad del Pais Vasco
Apdo 1072, 20080 San Sebastian (Spain)

[c] Dr. A. M. Martinez-Villacorta, Dr. A. Escobar, Prof. S. Moya
Soft Matter Nanotechnology Lab, CIC biomaGUNE
Paseo Miramón 182, 20014 Donostia-San Sebastián, Gipuzkoa (Spain)

Supporting information and the ORCID identification number(s) for the author(s) of this article can be found under <https://doi.org/10.1002/chem.201800418>.



Scheme 1. Inter-relations between the CpFe (benzene) structures involved in the reduction of metal salt precursors of metal NPs.



Scheme 2. Interactions between the cobalt sandwich complexes involved in the reduction of metal salts of metal salt precursors of metal NPs.

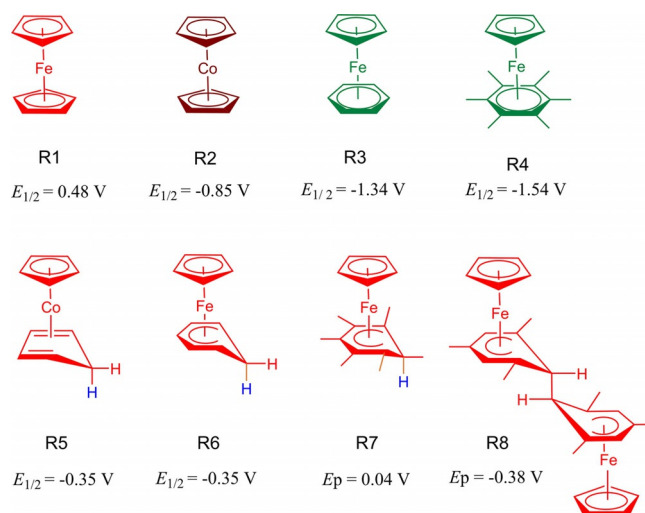
distance, slow electron transfer), leading to the formation of large NPs, which therefore cannot be competitive in catalysis. All these organometallic complexes are used here to reduce HAuCl_4 and K_2PdCl_4 , and the AuNPs^[12] and PdNPs^[13] formed are subsequently characterized. Their formation is discussed as a function of the nature and driving force,^[13] steric constraints, and other factors provided by the organometallic reductant, and these NPs are examined as catalysts in the reduction of 4-nitrophenol by NaBH_4 ^[14] (AuNPs and PdNPs) and Suzuki–Miyaura cross C–C coupling reactions (PdNPs).^[15]

Results and Discussion

We first examine the characteristics of the organometallic reductants, in particular with the use of cyclic voltammetry. We then investigate the AuNP and PdNP syntheses and finally the reactions catalyzed by these NPs, before concluding by comparing the qualities of the reductants. To follow the discussion, note that the NPs bear the same numbers as their organometallic precursors in Figure 1. For instance $\text{Au}^{\text{III}} + \text{R1}$ gives Au1, and so on.

Electron-reservoir and hydride-reservoir reductants

Known neutral electron-reservoir and hydride-reservoir organometallic reducing agents with iron^[5,8,10] and cobalt^[11] sandwich structures were chosen as reductants of late TM salts to generate catalytically active late TMNPs. These organometallic reduc-



Redox potentials: $E_{1/2}$: R4 < R3 < R2 < R6 = R5 < R1

Au NPs Sizes: Au1 > Au3 > Au8 > Au5 > Au6 > Au4 > Au2 > Au7

Pd NPs Sizes: Pd8 > Pd7 > Pd4 > Pd5 > Pd3 > Pd1 > Pd6 = Pd2

4-NP k_{app} (Au): Au5 > Au6 > Au1 > Au7 > Au8 > Au3 > Au2 > Au4

4-NP k_{app} (Pd): Pd5 > Pd6 > Pd7 > Pd8 > Pd1 > Pd2 = Pd4 > Pd3

Suzuki–Miyaura (Pd): Pd5 > Pd7 > Pd6 > Pd1 > Pd8 > Pd3 > Pd2 > Pd4

Figure 1. Various neutral electron-reservoir and hydride-reservoir organometallic sandwich complexes, denoted R1 to R8, used for the reduction of Au^{III} and Pd^{II} to AuNPs and PdNPs, respectively, their potentials $E_{1/2}$ of reversible oxidation (or E_p for irreversible oxidation), ranking of the TMNP sizes obtained using these reductants, and ranking of the TMNP efficiencies in the catalysis of 4-nitrophenol reduction (rate constants k_{app} with AuNPs and PdNPs) and Suzuki–Miyaura cross C–C coupling reactions (TONs with PdNPs). The nanoparticles are denoted by the atom (Au or Pd) followed by the same number as the number n of the reductant R_n used for their synthesis.

tants are the three 19-electron complexes of Fe and Co (electron reservoirs R2, R3, and R4) and three hydride-reservoir compounds of closely related structures (hydride reservoirs R5, R6, and R7). We wished to compare single-electron donors and single-hydride donors yielding, after reaction, the same cationic full sandwich structure. In addition, an organometallic dimer R8^[16] was included in the series of reductants, because it also provides a cationic sandwich complex similarly to the electron-reservoir and hydride-reservoir complexes after oxidation. Finally, ferrocene^[10b,17] was also compared with the more electron-rich complexes to examine the influence of the reaction driving force with the same metallocenic molecular structure. In Figure 1, these reductants are represented with their oxidation potentials (from Refs. [5], [18], [19], or new cyclic voltammetry measurements). At the bottom of Figure 1, the reducing power ranking is shown. The ranking of the catalytic efficiencies of the TMNPs synthesized with these reductants was further determined in the present work in the reduction of 4-nitrophenol (AuNPs and PdNPs) and the Suzuki–Miyaura reaction (PdNPs). The numbers indicated for the TMNPs correspond to those of the reductants used for their synthesis (Figure 1).

The redox potentials indicated in Figure 1 are exclusively the oxidation potentials of the neutral organometallic compounds. These values were recorded using decamethylferrocene (FeCp^*_2) as the internal reference^[20] or another permethylated

sandwich compound as reference with the measured potential in the same region as decamethylferrocene.^[20b] All the redox potential values are indicated versus $\text{FeCp}^*_{2,2}$.^[20] The cyclic voltammetry (CV) of complexes R5, R6, R7, and R8 that had not been reported earlier and were recorded specifically for the present study are given in Figure 2 a–d for R5–R8, respectively. The oxidation potentials of R1, R2, R3, and R4 are known,^[5,17,18] and they are recorded here as well as in Figure 2a–d with values that are found to be analogous to those reported in the literature.

The CV of R5 in DMF (Figure 2a) shows a partly chemically reversible wave at -0.35 V versus $\text{FeCp}^*_{2,2}$. At this scan rate (0.2 V s^{-1}), the 17-electron species formed upon monoelectronic oxidation of R5 is shown on the CV to decompose partly with cleavage of a C–H bond of the methylene group, to give

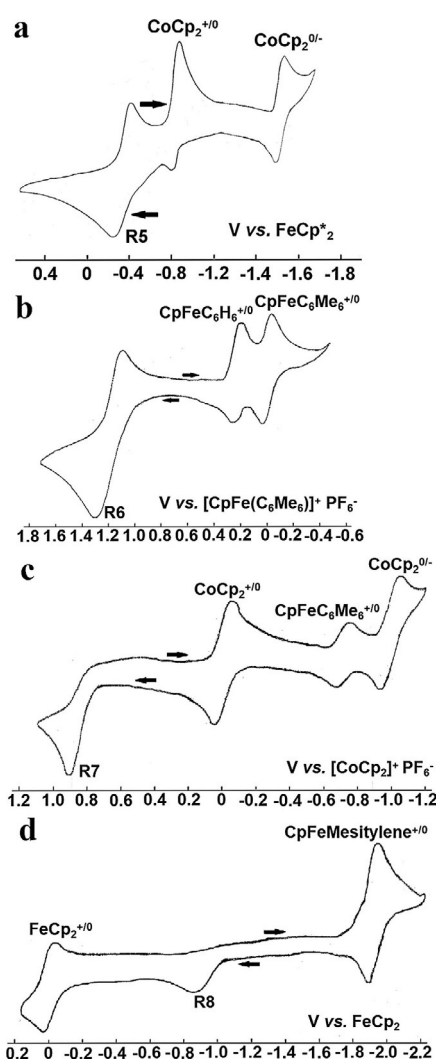


Figure 2. a) CV of R5. Internal reference: $\text{FeCp}^*_{2,2}$. b) CV of R6. Internal reference: $[\text{CpFeC}_6\text{Me}_6][\text{PF}_6]$; $E_{1/2}$ (R6) vs. $E_{1/2}$ ($[\text{CpFeC}_6\text{Me}_6][\text{PF}_6]$) = 1.19 V; $E_{1/2}$ ($[\text{CpFeC}_6\text{Me}_6][\text{PF}_6]$) vs. $E_{1/2}$ ($\text{FeCp}^*_{2,2}$) = -1.54 V, so $E_{1/2}$ (R6) = -0.35 V. c) CV of R7. Internal reference: $[\text{CoCp}_2][\text{PF}_6]$; E_p (R7) vs. $E_{1/2}$ ($[\text{CoCp}_2][\text{PF}_6]$) = 0.89 V, $E_{1/2}$ ($[\text{CoCp}_2][\text{PF}_6]$) vs. $E_{1/2}$ ($\text{FeCp}^*_{2,2}$) = -0.85 V, so E_p (R7) = 0.04 V. d) CV of R8. Internal reference: ferrocene; E_p (R8) vs. $E_{1/2}$ (ferrocene) = -0.86 mV, $E_{1/2}$ (ferrocene) vs. $E_{1/2}$ ($\text{FeCp}^*_{2,2}$) = 0.48 mV, so E_p (R8) = -0.38 mV. Solvent: DMF; 298 K; reference electrode: Ag; working and counter electrodes: Pt; scan rate: 0.2 V s^{-1} ; supporting electrolyte: $[\text{nBu}_4\text{N}][\text{PF}_6]$ (0.1 M).

back the 18-electron cobalticinium cation. The two CV waves of the latter ($\text{Co}^{\text{III/II}}$ and $\text{Co}^{\text{II/I}}$) are electrochemically reversible, as reported by Geiger.^[18] This CV shows the relatively fast oxidation of R5, but the partial chemical reversibility allows access to the $E_{1/2}$ redox potential.^[21]

The CV of R6 (Figure 2b) shows a very similar situation to that of R5, that is, the CV wave of R6 is partly chemically reversible, allowing both the determination of the $E_{1/2}$ redox potential of R6 at -0.35 V versus $\text{FeCp}^*_{2,2}$, and observation of the decomposition product R3^+ (presumably formed by *exo*-cyclic C–H bond cleavage by comparison to the oxidation of R7, *vide infra*), which appears as an electrochemically reversible wave of $\text{R3}^{+/0}$. The $E_{1/2}$ values are accessible using the internal reference R4^+ as its PF_6^- salt.

The CV of R7 (Figure 2c) shows an essential difference from that of its parent analogue R6, in that the CV wave of R7 is completely irreversible at the working scan rates up to 1 V s^{-1} . This indicates that the decomposition of R7 by *exo*-cyclic C–H bond cleavage to form R4^+ is much faster than that of R6. The result is the same in both cases R6 and R7, however, in that the oxidation product is observed in the CV as a reversible wave. For R7, this oxidation product is R4^+ . A convenient internal reference in this case was cobalticinium R2^+ introduced as the PF_6^- salt.

The CV of R8 (Figure 2d), similarly to that of R7, shows an irreversible wave and the appearance of a reversible wave for the oxidation product $[\text{FeCp}(\eta^6\text{-mesitylene})]^+$,^[10] resulting from *exo*-cyclic C–C bond cleavage in R8 following oxidation, with the bond cleavage faster than the electrochemical timescale. It is difficult to state whether C–C cleavage occurs after the first or the second monoelectronic anodic oxidation, but the oxidation wave of R8 is very broad, which favors the second hypothesis, with an electrostatic factor provoking the second monoelectronic oxidation at a more positive potential than the first.

The knowledge of the oxidation potential order, $\text{R4} > \text{R3} > \text{R2} > \text{R8} > \text{R6} = \text{R5} > \text{R7} > \text{R1}$, will be useful in examining the influence of the driving force of the reductant on the AuNP and PdNP sizes and catalytic efficiencies.

Synthesis and characterization of the AuNPs and PdNPs

HAuCl_4 and K_2PdCl_4 were reduced by the organometallic reductants R1–R8 to examine the influence of the characteristics of these reductants on the sizes and catalytic efficiencies of the TMNPs formed in this way. The reductant stoichiometry in the reduction of HAuCl_4 and K_2PdCl_4 matches that of the chloride numbers in the precursor. In the case of AuNPs and PdNPs obtained by reduction using R2 (for details, see Experimental Section), the four required equivalents of CoCp_2 were injected quickly into the aqueous solution of precursor $[\text{HAuCl}_4 \cdot 3\text{H}_2\text{O}]$ (1 mg) or K_2PdCl_4 (0.83 mg), $2.54 \times 10^{-3} \text{ mmol}$ and poly(vinylpyrrolidone) (PVP 10000) under N_2 at RT. The solution color changed immediately after reactant mixing, indicating the formation of TMNPs. The TMNPs were further named Aux and Pdy, with x or y denoting the number of the organometallic precursor Rx or Ry in Figure 1. The UV/Vis spectra of these TMNPs are shown in Figure 6 and Figures S2–S8 and S27 (Sup-

porting Information). For example, the UV/Vis spectrum of Au2 shows both the surface plasmon band (SPB)^[12] at 500 nm, characteristic of the Au2 core, and the cobalticinium absorption at 393 nm, which is also observed in Pd2. In all cases, metalloccinium absorptions are present in the UV/Vis spectra, showing that all the organometallic reductants are oxidized by the metal cations to form the metallocciniums and the metal(0) NPs, in accord with the favorable driving forces and with the CV studies.

Au7, which showed the smallest and best dispersed NPs among all the AuNPs according to the TEM (see below), was chosen for XPS measurements. The Au4f_{7/2} peak of Au7 in the XPS spectrum (Figure 3) at around 83.3 eV is assigned to Au⁰, which is confirmed by the AuNP SPB. The XPS of Pd7 reduced by the same reductant (R7) shows that there is approximately 51% Pd⁰ and 49% Pd^{II}.

All the TMNPs were characterized by TEM (Figures 4 and 5; see Figures S9, S10, Supporting Information, for the histograms). R1 (ferrocene)^[17] is the weakest reductant among the

organometallic reductants R1–R8,^[18] and therefore, not surprisingly, large AuNPs are formed with R1. Au1 NPs were obtained with an average size of 19 nm. Except for Au1, however, it is difficult to establish a correlation between the driving force and the AuNP core size. Concerning the PdNPs, the driving force and nature, that is, electron reservoir versus hydride reservoir, does not seem to have any significant influence on the PdNP core size, which is between 3.0 and 3.8 nm; only the bulk of the reductant appears to be responsible for the formation of relatively large PdNPs in the cases of R7 (Pd7: 4.7 nm) and R8 (Pd8: 9.1 nm). The reaction between R1 and Au^{III} appears to be relatively fast, however. Conversely, no color change was observed upon injection of R1 into aqueous K₂PdCl₄; the blue color corresponding to ferricinium appeared after 1 h, indicating that more than 1 h is required to obtain the Pd1 NPs.

Comparison of catalytic efficiencies of AuNPs and PdNPs for 4-nitrophenol reduction

The reduction of nitroaromatics, including nitrophenols, which are toxic and anthropogenic, to aminoaromatics, which are very useful for a wealth of applications, is an essential TM-catalyzed redox reaction.^[14,22,23] In particular, the reduction of 4-nitrophenol (4-NP) to 4-aminophenol (4-AP) by NaBH₄ is a model reaction allowing the evaluation of the activity of the catalyst surface.^[14] The absorption of 4-NPate in the UV/Vis spectra at 400 nm thus facilitates the observation of the reaction kinetics by following the decrease of this band, whereas the increase in the absorption band at 300 nm shows the formation of 4-AP. The AuNPs (0.5 mol% Au) or PdNPs (0.02 mol% Pd) were

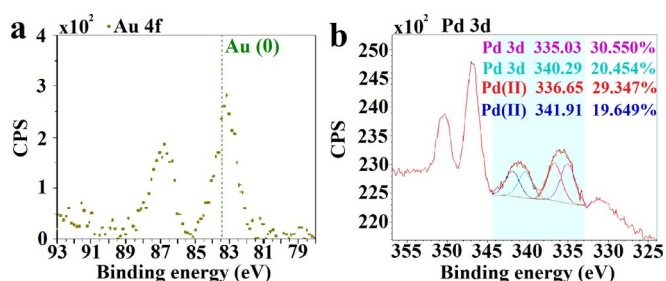


Figure 3. X-ray photoelectron spectroscopy of a) Au7 and b) Pd7 NPs.

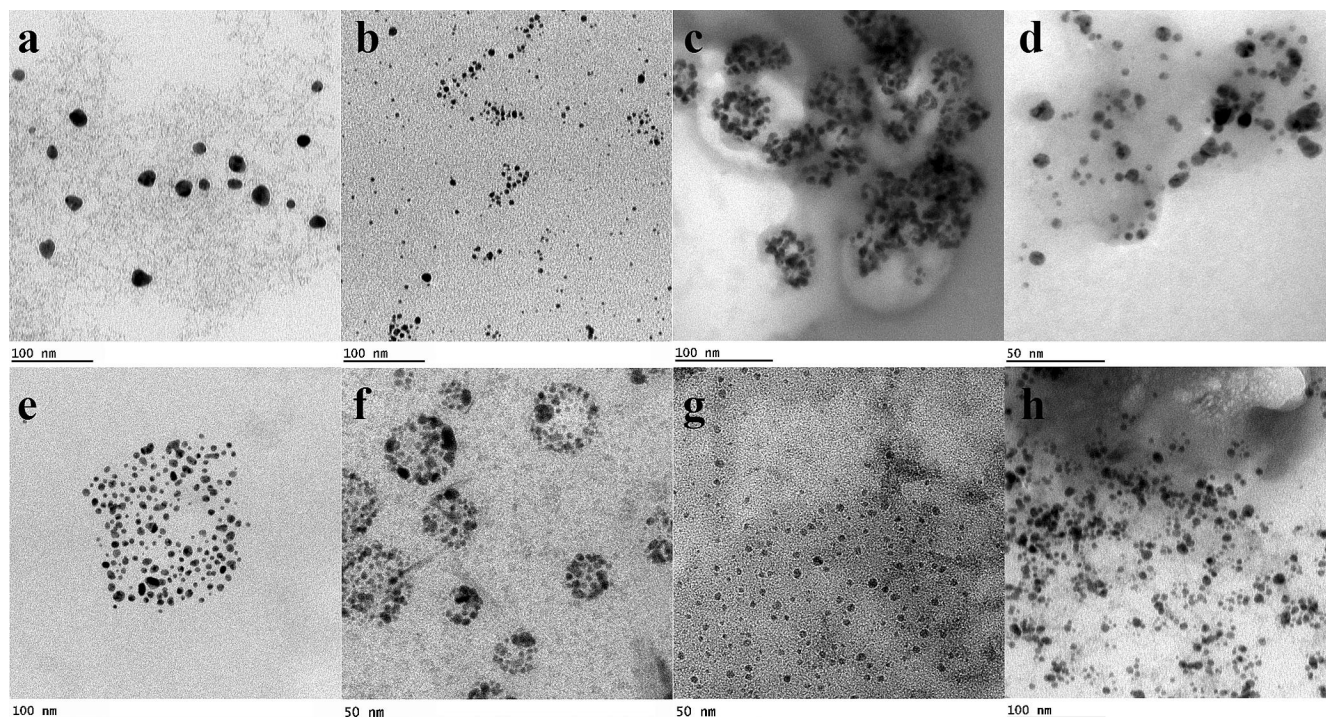


Figure 4. TEM pictures of AuNPs: a) Au1; b) Au2; c) Au3; d) Au4; e) Au5; f) Au6; g) Au7; h) Au8.

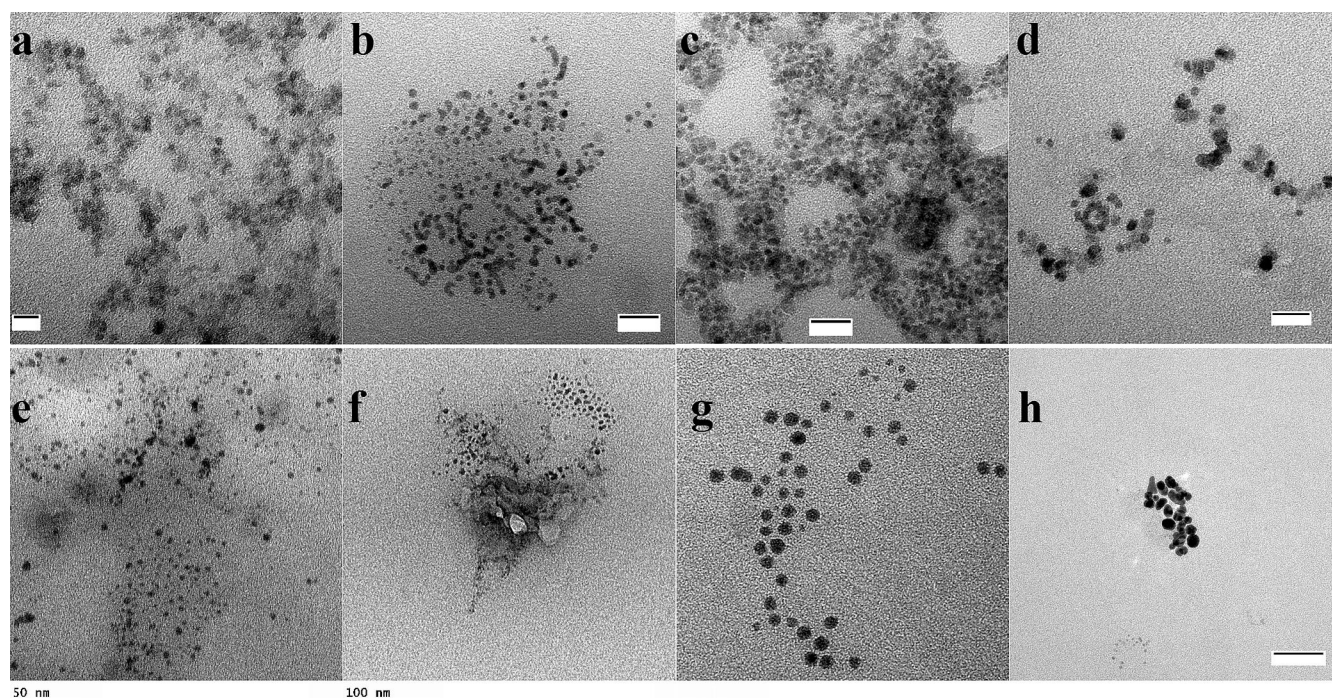


Figure 5. TEM pictures of PdNPs: a) Pd1 (scale bar: 10 nm); b) Pd2 (scale bar: 20 nm); c) Pd3 (scale bar: 20 nm); d) Pd4 (scale bar: 15 nm); e) Pd5; f) Pd6; g) Pd7 (scale bar: 20 nm); h) Pd8 (scale bar: 50 nm).

added according to the procedure described in the Experimental Section, and the reactions were monitored by UV/Vis spectroscopy (Figures S11–S26, Supporting Information). The kinetic rate constants for this reaction follow the equation $k_{app} \times t = -\ln(C_t/C_0)$, and are shown in Table 1. The value of k_{app} decreases in the order Au5 > Au6 > Au1 > Au7 > Au8 > Au3 > Au2 > Au4 and Pd5 > Pd6 > Pd7 > Pd8 > Pd1 > Pd2 = Pd4 > Pd3. The TMNPs Au5 and Pd5 obtained from R5 are therefore the most

efficient catalysts. In addition, no induction times are observed in all cases, and the PdNPs work better than the AuNPs. Pd5, with an average particle size of 3.5 nm, exhibits the highest reaction rate, $k_{app} = 38 \times 10^{-3} \text{ s}^{-1}$, with 200 ppm catalytic metal, which is the most efficient catalyst compared with recent literature concerning AuNP and PdNP catalysis in 4-NP reduction reactions (Table 2).

Even though Au1 is large (19 nm), it performs well and exhibits a higher reaction rate ($k_{app} = 15 \times 10^{-3} \text{ s}^{-1}$) than some Au NPs of smaller size (for instance, Au7, Au8, Au3, Au2, Au4) in the 4-NP reduction reaction. Remarkably, if ferricinium chloride is removed from the Au1 surface by dialysis (Figure 6 b, noted Au1-1), however, Au1-1 loses its activity in the reaction (no reaction in 6 h), although its SPB changes only from 600 for Au1 to 586 nm after dialysis in Au1. Then no clear color change appears, because the color is dominated by the blue plasmonic absorption, even if in the same time the absorption at 616 nm corresponding to ferricinium, which is hidden by the broad Au SPB band, is removed upon dialysis. Upon dialysis of Pd1 to Pd1-1 (Figure S27, Supporting Information), however, the color changes from green (owing to ferricinium) to faint yellow, and the clear disappearance of the ferricinium absorption in the UV/Vis spectrum is characteristic of the removal of ferricinium. Interestingly, the average AuNP core size does not change significantly from Au1 to Au1-1 (Figure S28, Supporting Information), indicating that the removal of ferricinium chloride and cancelling of catalytic properties in 4-NP reduction upon dialysis does not influence the AuNP core size. Although the reaction mechanism of 4-NP reduction is not precisely known,^[14] Ballauff's group suggested rearrangement of the substrates 4-NP and NaBH₄ at the NPs surface on the basis of the Lang-

Table 1. 4-NP reduction by NaBH₄ catalyzed by TMNPs in water at 20 °C.

Catalyst	Amount ^[a] [mol %]	D_{core} ^[b] [nm]	t_0 ^[c] [s]	k_{app} ^[d] [10^{-3} s^{-1}]
Au1	0.5	18.83	0	15.0
Au1-1	0.5	17.38	–	–
Au2	0.5	4.19	0	4.75
Au3	0.5	6.82	0	7.87
Au4	0.5	4.47	0	3.26
Au5	0.5	5.15	0	22.7
Au6	0.5	4.77	0	17.4
Au7	0.5	3.59	0	12.5
Au8	0.5	5.75	0	8.84
Pd1	0.02	3.26	0	14.6
Pd2	0.02	2.99	0	11.3
Pd3	0.02	3.31	0	7.56
Pd4	0.02	3.83	0	11.3
Pd5	0.02	3.47	0	38.0
Pd6	0.02	2.99	0	21.3
Pd7	0.02	4.72	0	16.9
Pd8	0.02	9.02	0	15.8

[a] Amount of catalysts used in the catalyzed 4-NP reduction. NaBH₄ is in excess (81 equiv.). [b] Core size (TEM) of the TMNPs. [c] Induction time. [d] Rate constant.

Table 2. Comparison of 4-NP reduction by NaBH₄ using various Pd and Au NP catalysts in recent literature.

Catalysts	Stabilizer	Catalyst amount [mol %]	NaBH ₄ [equiv]	k _{app} [10 ⁻³ s ⁻¹]	Ref.
Pd NPs	PVP10 000	0.02	81	38	this work
	PEDOT-PPS	77	excess	65.8	[24]
	CeO ₂	0.56	83	8	[25]
	G0–27 TEG dendrimer	0.2	100	4	[26]
	CNT/PiHP	4	80	5	[27]
	Fe ₃ O ₄	10	139	33	[28]
	microgels	2.1	100	1.5	[29]
	Ppy/TiO ₂	2.6	11	12.2	[30]
	SBA-15	100	1000	12	[31]
	SPB	0.36	100	4.41	[22], [32]
	glycodendrimers	0.2	81	4.4	[33]
	tristrz-PEG2000	0.2	81	24.8	[34]
	PEG2000	0.2	81	16.9	[35]
	Au NPs	tristrz-PEG2000	0.2	81	43.7
PEG2000		0.2	81	15.8	[35]
DMF		15	2000	7	[36]
CTAB		1.25	500	6.1	[37]
PEO-b-PAA		0.5	300	9.5	[38]
PVP		1.56	147	10.2	[39]
cyclodextrin		17.6	44	4.56	[40]
polyaniline		17.6	44	11.7	[41]
methyl-imidazolium-based ionic polymer		20	88	33	[42]
PAMAM		0.1	100	7.91	[43]
PPI		0.1	100	14.7	[44]
dendritic 1,2,3-triazole terminated with peg2000		0.5	80	7	[45]
Fc ⁺ -trz-Cl ⁻		0.5	80	1.1	[46]
mono-trz-PEG2000		0.2	81	14	[47]
nano-PEG550		0.2	81	7.5	[47]
polymer trz-PEG		0.2	81	11	[47]
NaBH ₄		1	100	20	[3b]
Abroma augusta Linnbark extract		4.3	300	7	[48]
1,4-bis(terpyridine-4-yl) benzene		not provided (0.5 mg catalyst)	100	1.9	[49]
GO@NH ₂		4.5	80	35.6	[50]
Fe ₂ O ₃ -GO		5	50	4.2	[51]
triazoletemini PEO	0.5	81	5.2	[52]	

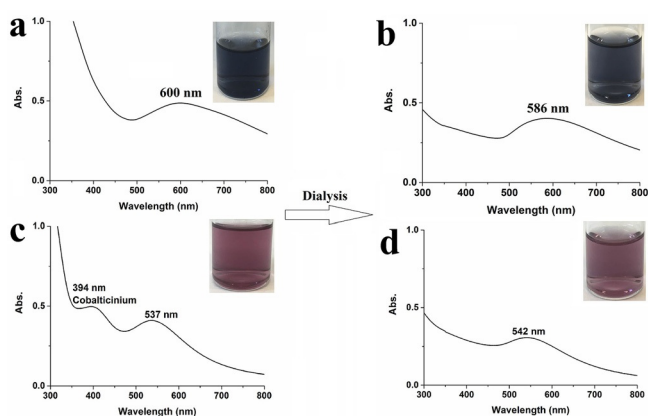


Figure 6. UV/Vis spectra and photographs of Au1 and Au5 before (a and c) and Au1-1 and Au5-1 after (b and d) dialysis.

muir–Hinshelwood (LH) kinetic model.^[22] Ferricinium appears to be an excellent electrostatic stabilizer, which, using its large bulk, protects the core surface from inhibition by the PVP polymer. If ferricinium is close to the surface, it is not bonded to it, allowing easy approach and binding by the substrate and hy-

dride, and the PVP stabilizer appears to be remote from the surface, which allows free approach of the substrate and hydride. On the other hand, in the absence of ferricinium, the PVP binds the AuNP core surface directly, provoking inhibition of the catalysis of 4-NP reduction.

The effect of cobalticinium in this reaction was researched with the best Au5 NPs upon dialysis (Figure 6c,d). Following this process, the UV/Vis absorption at 394 nm (cobalticinium) is missing, which indicates that cobalticinium is also removed by dialysis. Then the NPs become PVP-stabilized Au5-1. Even though the SPB and color do not change much, the k_{app} value of the 4-NP reduction reaction decreases from 22.7 × 10⁻³ s⁻¹ (Au5) to 3.1 × 10⁻³ s⁻¹ (Au5-1) with the same catalytic amount (Figure S29, Supporting Information). The disappearance of the electrostatically protecting metallocenium upon dialysis provokes the cancellation or decrease of the catalytic properties of the AuNPs, which shows the unique role of the metallocenium in NP catalysis. It also illustrates the fact that approach to the NP core surface is crucial for the catalytic reaction and is facilitated by the presence of the metallocenium cation.

Comparison of catalytic efficiency of PdNPs for the Suzuki–Miyaura coupling reaction

The catalytic activities of PdNPs were examined in one of the representative Pd-catalyzed reactions, the Suzuki–Miyaura cross C–C bond coupling, which plays a key role in the construction of carbon backbones and has attracted research interest with extensive applications in organic synthesis.^[15] The amounts of Pd catalysts reported in the literature are very variable, and there are several examples of Suzuki–Miyaura reactions reported with catalyst amounts of the order of parts per million.^[53]

Indeed, the minimization of the amount of Pd catalyst in these reactions is an essential goal toward possible applications in industrial synthesis. Another key parameter for “green chemistry” is the avoidance of the use of toxic and expensive ligands such as phosphines, which are often found in organometallic catalysts. This is achieved well with PdNPs, especially if they are used in very small amounts. PVP-stabilized Pd1–Pd8 NPs are utilized here to catalyze the Suzuki–Miyaura reaction between bromobenzene and phenylboronic acid at 80 °C under N₂ with 300 ppm Pd catalyst (Table 3). The three PdNPs synthesized from the hydride reservoirs R5, R6, and R7 are the three best catalysts in the series, with Pd5 again the best catalyst. Pd5 catalyzes the Suzuki–Miyaura cross C–C bond coupling between bromobenzene and phenylboronic acid with 99% isolated yield and a TOF of 13.8 h⁻¹ (Table 3).

From the comparison of all the AuNPs and PdNPs in the 4-NP reduction and Suzuki–Miyaura reactions, Au5 and Pd5 always show the best activities. On the other hand, the activities of Au2 and Pd2 are rather poor. R2 is a stronger electron-transfer reductant than R5 according to the CV data, and the NP size orders Au2 < Au5 and Pd2 < Pd5 (Figures 4 and 5) are fully consistent with the order of the driving forces. The oxidized form of R2 and R5 is the same, for example, cobalticinium (Figure 2a, and Figures S2 and S5, Supporting Information), showing that the hydride reservoirs give better results than electron reservoirs for the catalytic activity of AuNPs and PdNPs in these catalytic reactions. A possible explanation is that hydride reservoirs transfer hydrides to transition metal cat-

ions, which is followed by fast reductive elimination to metal(0), and further hydride transfer makes the NP surface very reactive. On the other hand, electron transfer to cationic transition metals is followed by more significant structural reorganization before the metal(0) state is reached.

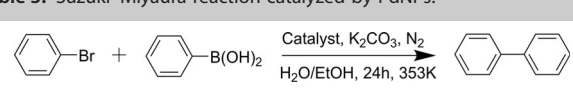
Conclusions

The parameters of the organometallic reductants of HAuCl₄ and K₂PdCl₄ to form AuNPs and PdNPs, including driving force, bulk, and electron- versus hydride-reservoir nature, have been scrutinized for their potential influence on the catalytic efficiency. The hydride-reservoir complexes [CoCp(η⁴-C₅H₆)], [FeCp(η⁵-C₆H₇)], and [FeCp(η⁵-C₆H₆H)] are shown here to form AuNPs and PdNPs in the presence of PVP, giving better catalytic results than those formed using the electron-reservoir complexes FeCp₂, CoCp₂, [FeCp(η⁶-C₆H₆)], and [FeCp(η⁶-C₆Me₆)] under the same conditions. The best results for both 4-nitrophenol reduction by NaBH₄ and Suzuki–Miyaura cross C–C coupling are obtained with AuNPs and PdNPs synthesized through reduction of the precursors HAuCl₄ and K₂PdCl₄ by [CoCp(η⁴-C₅H₆)]. For the former reaction, the PdNPs are somewhat more efficient than the AuNPs. Indeed, the PdNPs obtained from this complex show the high reaction rate constant $k_{app} = 38 \times 10^{-3} \text{ s}^{-1}$ with 200 ppm catalyst. This data shows that it is the most efficient catalyst compared with recent literature concerning AuNPs and PdNPs in the catalysis of 4-NP reduction. These PdNPs also catalyze the Suzuki–Miyaura coupling between bromobenzene and phenylboronic acid with 99% isolated yield and a TOF of 13.8 h⁻¹. The bulky reductants R4 and R7 with a permethylated ring and the dimer R8 give less satisfactory catalytic efficiencies than the parent complexes, apparently because of steric problems around the NP core. The presence of the PVP stabilizer in the NP synthesis decreases the catalytic activities of the NP catalysis considerably. The presence of the cationic sandwich complex that surrounds the NP cores is responsible for the high catalytic efficiency, seemingly because the sandwich salt inhibits close contact between the PVP polymer and the NP core. Meanwhile, a certain proportion of the chloride counter anions of the cationic sandwich units are coordinated to the AuNP core. For instance, dialysis of the NPs removes the metallocenium chloride, leaving the PVP-stabilized NP core size unchanged, and these metallocenium-free AuNPs then show a loss of or decrease in the catalytic efficiency. This shows that the carefully optimized mode of NP synthesis is excellent and very efficient for catalytic applications. Note that all the organometallic sandwich complexes surrounding the NPs have absolutely no catalytic activities by themselves, because they are robust 18-electron cationic complexes that do not undergo any decoordination to active 16-electron species.^[10c]

Experimental Section

Tetrahydrofuran (THF) and pentane were heated at reflux and freshly distilled, and milli-Q water (18.2 MΩ) was used for all the NP preparations.

Table 3. Suzuki–Miyaura reaction catalyzed by PdNPs.^[a]



Catalysts	Conversion [%] ^[b]	Yield [%] ^[c]	TON	TOF [h ⁻¹]
Pd1	58	52	173.3	7.2
Pd2	30	26	86.7	3.6
Pd3	32	27	90	3.8
Pd4	15	10	33.3	1.4
Pd5	100	99	330	13.8
Pd6	70	64	213.3	8.9
Pd7	87	81	270	11.3
Pd8	45	42	140	5.8

[a] Reaction conditions: bromobenzene (0.5 mmol), phenylboronic acid (0.75 mmol), K₂CO₃ (1 mmol), 300 ppm catalysts, H₂O/EtOH: 1:1 mL, 80 °C, 24 h, under N₂. [b] ¹H NMR conversion. [c] Isolated yield.

Synthesis of Au and Pd nanoparticles

From 19e sandwich complexes; example of R2: In a Schlenk flask, Na/Hg amalgam was prepared in dry THF under N₂ at RT. Then, cobalticenium hexafluorophosphate [CoCp₂][PF₆] (Cp = η⁵-C₅H₅) (50 mg) and THF (20 mL) were added, and the mixture was stirred for 2 h. The solution changed color progressively from yellow to brown, indicating the formation of cobaltocene [CoCp₂]. The solvent was removed in vacuo, providing the crude product, which was redissolved in pentane to eliminate the insoluble NaPF₆ salt by cannula filtration.

Finally, pentane was removed in vacuo, and the product was redissolved again in dry THF (20 mL) for further use. HAuCl₄·3H₂O (1 mg, 2.54 × 10⁻³ mmol) or K₂PdCl₄ (0.83 mg, 2.54 × 10⁻³ mmol) and PVP10000 (2 equiv.) were dissolved in 20 mL milli-Q water under nitrogen in a standard Schlenk flask and stirred for 30 min. Then a fresh [CoCp₂] solution (4 equiv.) was injected quickly into the Schlenk flask, and the color change of the solution indicated the formation of the NPs Au₂ or Pd₂.

The syntheses of AuNPs and PdNPs from the other 19e sandwich compounds [FeCp(η⁶-C₆H₆)] (R3, synthesized from [FeCp(η⁶-C₆H₆)] [PF₆] as starting materials at 0 °C) and [FeCp(η⁶-C₆Me₆)] (R4, synthesized from [FeCp(η⁶-C₆Me₆)] [PF₆] as starting materials at RT), and from ferrocene (R1, used as purchased) were performed in a similar way, except that the reaction between R1, K₂PdCl₄, and PVP-1000 required stirring for 2 h to form the Pd1 NPs.

From hydride-reservoir sandwich complexes; example of R5: Cobalticenium hexafluorophosphate [CoCp₂][PF₆] (Cp = η⁵-C₅H₅) (50 mg) and THF (20 mL) were added in a Schlenk flask under N₂ at RT. Then, NaBH₄ (5 equiv.) was added, and the mixture was stirred for 2 h. The solution changed color progressively from yellow to red, indicating the formation of R5. The solvent was removed in vacuo, providing the crude product, which was redissolved in pentane to eliminate the insoluble NaPF₆ salt by cannula filtration. Finally, pentane was removed in vacuo, and the product was redissolved again in dry THF (20 mL) for further use.

HAuCl₄·3H₂O (1 mg, 2.54 × 10⁻³ mmol) or K₂PdCl₄ (0.83 mg, 2.54 × 10⁻³ mmol) and PVP10000 (2 equiv.) were dissolved in Milli-Q water (20 mL) under nitrogen in a standard Schlenk flask and stirred for 30 min. Then, a fresh R5 solution (4 equiv.) was injected quickly into the Schlenk flask, and the color change of the solution indicated the formation of Au₅ or Pd₅ nanoparticles.

Au and Pd NPs were formed similarly from other H-donor sandwich compounds, R6 (synthesized from [FeCp(η⁶-C₆H₆)] [PF₆] as starting materials at 0 °C) and R7 (synthesized from [CpFe(η⁶-C₆Me₆)] [PF₆] as starting materials at 50 °C).

From the dimer R8: In a Schlenk flask, Na/Hg amalgam was prepared in dry THF under N₂ at RT. Then, [CpFe(η⁶-mesitylene)] [PF₆] (50 mg) and THF (20 mL) were added, and the mixture was stirred for 2 h at 0 °C. The solution changed color progressively from yellow to forest green, indicating the formation of [CpFe(η⁶-mesitylene)]. The solvent was removed in vacuo, providing the crude product, which was redissolved in pentane to eliminate the insoluble NaPF₆ salt by cannula filtration. Then, the pentane solution was kept overnight to allow spontaneous dimerization to occur. Finally, pentane was removed in vacuo, and the red product (R8) was redissolved in dry THF (20 mL) for further use.

HAuCl₄·3H₂O (1 mg, 2.54 × 10⁻³ mmol) or K₂PdCl₄ (0.83 mg, 2.54 × 10⁻³ mmol) and PVP10000 (2 equiv.) were dissolved in milli-Q water (20 mL) under nitrogen in a standard Schlenk flask and stirred for 30 min. Then, a fresh R8 solution (4 equiv.) was injected quickly into the Schlenk flask, and the color change of the solution indicated the formation of Au₈ or Pd₈ NPs.

Reduction of 4-NP by NaBH₄ (at 20 °C)

Generally, 4-NP (1 equiv.) was mixed with excess NaBH₄ (81 equiv.) in water under air. The color of the solution changed from light yellow to dark yellow owing to the formation of the 4-nitrophenolate ion. Then, a solution containing AuNPs (0.5 mol%) or Pd NPs (200 ppm) was added to the mixture. The solution quickly lost its dark yellow color with time, and the progress of the reaction was monitored by UV/Vis spectroscopy (40 s for each run).

Suzuki–Miyaura reaction catalyzed by PdNPs

A dry Schlenk flask was charged with phenylboronic acid (0.75 mmol), bromobenzene (0.5 mmol), and K₂CO₃ (1 mmol). Catalytic amounts of a solution of PdNPs were added successively, then H₂O and EtOH were added to make a total solvent volume of 2 mL (H₂O/EtOH = 1:1, vol/vol). The suspension was then allowed to stir under N₂ for 24 h at 80 °C. After the reaction, the Schlenk flask was cooled to RT, the mixture was extracted three times with diethyl ether (3 × 20 mL), the organic phase was dried over Na₂SO₄, and the solvent was removed in vacuo. The crude product was checked by ¹H NMR to calculate the conversion. In parallel, the reaction was checked using TLC in only petroleum ether as eluent. Purification by flash chromatography column was conducted with silica gel as the stationary phase and petroleum ether as the mobile phase.

Acknowledgements

Financial support from the China Scholarship Council (CSC) of the People's Republic of China (grants to F.F. and Q.W.), the CNRS, and the Universities of Bordeaux and Basque Country at San Sebastian and CIC biomaGUNE at San Sebastian are gratefully acknowledged.

Conflict of interest

The authors declare no conflict of interest.

Keywords: catalysis · electron reservoir · hydride reservoir · nanoparticles · sandwich complexes

- [1] a) R. Ye, B. Yuan, J. Zhao, W. T. Ralston, C. Y. Wu, E. U. Bari, F. D. Toste, G. A. Somorjai, *J. Am. Chem. Soc.* **2016**, *138*, 8533–8537; b) M. Haruta, *Angew. Chem. Int. Ed.* **2014**, *53*, 52–56; *Angew. Chem.* **2014**, *126*, 54–58; c) M. Sankar, N. Dimitratos, P. J. Miedzak, P. P. Wells, C. J. Kiely, G. J. Hutchings, *Chem. Soc. Rev.* **2012**, *41*, 8099–8139; d) A. Corma, A. Leyva-Perez, J. M. Sabater, *Chem. Rev.* **2011**, *111*, 1657–1712; e) L. M. Bronstein, Z. B. Shifrina, *Chem. Rev.* **2011**, *111*, 5301–5344; f) V. S. Myers, M. G. Weier, E. V. Carino, D. F. Yancey, S. Pande, R. M. Crooks, *Chem. Sci.* **2011**, *2*, 1632–1646; g) A. Balanta, C. Godard, C. Claver, *Chem. Soc. Rev.* **2011**, *40*, 4973–4985; h) J.-M. Basset, R. Psaro, D. Roberto, R. Ugo, *Modern Surface Organometallic Chemistry*, Wiley-VCH, Weinheim, **2009**; i) V. Polshettiwar, R. S. Varma, *Green Chem.* **2010**, *12*, 743–754; j) D. Astruc, F. Lu, J. Ruiz, *Angew. Chem. Int. Ed.* **2005**, *44*, 7852–7872; *Angew. Chem.* **2005**, *117*, 8062–8083; k) M. T. Reetz, J. G. de Vries, *Chem. Commun.* **2004**, 1559–1563.
- [2] a) M. Brust, M. Walker, D. Bethel, D. J. Schiffrin, R. Whyman, *J. Chem. Soc. Chem. Commun.* **1994**, 801–802; b) Y. G. Sun, Y. N. Xia, *Nano Lett.* **2003**, *3*, 675–679; c) Y. P. Sun, X. Q. Li, J. S. Qao, W. X. Zhang, H. P. Wang, *Adv. Colloid Interface Sci.* **2006**, *120*, 47–56; d) M. P. Mallin, C. J. Murphy, *Nano Lett.* **2002**, *2*, 1235–1237; e) S. H. Chen, K. Kimura, *Langmuir* **1999**, *15*, 1075–1082; f) Y. M. Mohan, K. Lee, T. Premkumar, K. E. Geckeler, *Polymer* **2007**, *48*, 158–164.

- [3] a) M. He, Q. Wang, R. Wang, Y. Xie, W. F. Zhao, C. S. Zhao, *ACS Appl. Mater. Interfaces* **2017**, *9*, 15962–15974; b) C. Deraedt, L. Salmon, S. Gatard, R. Ciganda, R. Hernandez, J. Ruiz, D. Astruc, *Chem. Commun.* **2014**, *50*, 14194–14196.
- [4] a) J. M. Yan, X. B. Xiang, S. Han, H. Shioyama, Q. Xu, *Angew. Chem. Int. Ed.* **2008**, *47*, 2287–2289; *Angew. Chem.* **2008**, *120*, 2319–2321; b) C. Schöttle, P. Bockstaller, R. Popescu, D. Gerthsen, C. Feldmann, *Angew. Chem. Int. Ed.* **2015**, *54*, 9866–9870; *Angew. Chem.* **2015**, *127*, 10004–10008; c) C. Schöttle, D. E. Doronkin, R. Popescu, D. Gerthsen, J. D. Grünwald, C. Feldmann, *Chem. Commun.* **2016**, *52*, 6316–6319.
- [5] a) J.-R. Hamon, D. Astruc, P. Michaud, *J. Am. Chem. Soc.* **1981**, *103*, 758–766; b) J. C. Green, M. R. Kelly, M. P. Payne, E. A. Seddon, D. Astruc, J.-R. Hamon, P. Michaud, *Organometallics* **1983**, *2*, 211–218; c) M. V. Rajasekharan, S. Giezynski, J. H. Ammeter, N. Oswald, J.-R. Hamon, P. Michaud, D. Astruc, *J. Am. Chem. Soc.* **1982**, *104*, 2400–2407; d) D. Astruc, *Acc. Chem. Res.* **1986**, *19*, 377–383.
- [6] A. Rapakousiou, C. Belin, L. Salmon, J. Ruiz, D. Astruc, *Chem. Commun.* **2017**, *53*, 6267–6270.
- [7] a) R. Ciganda, J. Irigoyen, D. Gregurec, R. Hernández, S. Moya, C. Wang, J. Ruiz, D. Astruc, *Inorg. Chem.* **2016**, *55*, 6361–6363; b) R. Ciganda, H. Gu, R. Hernández, A. Escobar, A. Martínez, L. Yate, S. Moya, J. Ruiz, D. Astruc, *Inorg. Chem.* **2017**, *56*, 2784–2791.
- [8] A. N. Nesmeyanov, N. A. Volkenau, I. N. Bolesova, *Dokl. Akad. Nauk SSSR* **1974**, *217*, 104–106.
- [9] a) D. Astruc, J.-R. Hamon, G. Althoff, E. Román, P. Batail, P. Michaud, J.-P. Mariot, F. Varret, D. Cozak, *J. Am. Chem. Soc.* **1979**, *101*, 5445–5447; b) C. Moinet, E. Román, D. Astruc, *J. Electroanal. Chem.* **1981**, *121*, 241–253.
- [10] a) I. U. Khand, P. L. Pauson, W. E. Watts, *J. Chem. Soc. C* **1968**, 2257–2259; b) For redox and hydride transfer reactions of organometallic sandwich complexes, see Ref. [10c], chapt. 12; c) D. Astruc, *Organometallic Chemistry and Catalysis*, Springer, Berlin, **2007**.
- [11] M. L. H. Green, L. Pratt, G. Wilkinson, *J. Chem. Soc.* **1959**, 3753–3767.
- [12] M.-C. Daniel, D. Astruc, *Chem. Rev.* **2004**, *104*, 293–346.
- [13] For an analysis of the role of the driving force in electron transfer reactions, see a) R. A. Marcus, N. Sutin, *Biochim. Biophys. Acta Rev. Bioenerg.* **1985**, *811*, 265–322; b) D. Astruc, *Electron Transfer and Radical Processes in Transition Metal Chemistry*, Wiley-VCH, New York, **1995**.
- [14] a) N. Pradhan, A. Pal, T. Pal, *Colloids Surf. A* **2002**, *196*, 247–257; b) P. Hervés, M. Perez-Lorenzo, L. M. Luiz-Marzan, J. Dzubielia, M. Ballauff, *Chem. Soc. Rev.* **2012**, *41*, 5577–5587; c) T. Aditya, A. Pal, T. Pal, *Chem. Commun.* **2015**, *51*, 9410–9431; d) P. Zhao, X. Feng, D. S. Huang, G. Y. Yang, D. Astruc, *Coord. Chem. Rev.* **2015**, *287*, 114–136.
- [15] a) N. Miyaura, A. Suzuki, *Chem. Rev.* **1995**, *95*, 2457–2483; b) A. Suzuki, in *Modern Arene Chemistry* (Ed.: D. Astruc), Wiley-VCH, Weinheim, **2002**, pp. 53.
- [16] A. N. Nesmeyanov, S. P. Solodovnikov, N. A. Vol'kenau, L. S. Kotesova, N. A. Sinitsina, *J. Organomet. Chem.* **1978**, *148*, C5–C7.
- [17] a) E. O. Fischer, W. Pfab, *Z. Naturforsch. B* **1952**, *7*, 377–379; b) G. Wilkinson, M. Rosenblum, M. C. Whiting, R. B. Woodward, *J. Am. Chem. Soc.* **1952**, *74*, 2125–2126.
- [18] N. G. Connelly, W. E. Geiger, *Chem. Rev.* **1996**, *96*, 877–910.
- [19] W. E. Geiger, *J. Am. Chem. Soc.* **1974**, *96*, 2632–2634.
- [20] a) I. Noviadri, K. N. Brown, D. S. Fleming, P. T. Gulyas, P. A. Lay, A. F. Masters, L. Phillips, *J. Phys. Chem. B* **1999**, *103*, 6713–6722; b) J. Ruiz Aranzas, M.-C. Daniel, D. Astruc, *Can. J. Chem.* **2006**, *84*, 288–299.
- [21] For chemical and electrochemical reversibilities of CV waves, see A. J. Bard, L. R. Faulkner, *Electrochemical Methods: Fundamentals and Applications*, 2nd ed., Ref. [13b], chapt. 1, Wiley, New York **2001**.
- [22] a) Y. Mei, Y. Lu, F. Polzer, M. Ballauff, M. Dreshler, *Chem. Mater.* **2007**, *19*, 1062–1069; b) S. Wunder, F. Polzer, Y. Lu, Y. Mei, M. Ballauff, *J. Phys. Chem. C* **2010**, *114*, 8814–8820; c) S. Wunder, Y. Lu, M. Albrecht, M. Ballauff, *ACS Catal.* **2011**, *1*, 908–916; d) Y. Lu, M. Ballauff, *Prog. Polym. Sci.* **2016**, *59*, 86–104.
- [23] a) J. Lee, J. Park, H. Song, *Adv. Mater.* **2008**, *20*, 1523–1528; b) Z. Zhang, C. Shao, P. Zou, P. Zhang, M. Zhang, J. Mu, Z. Guo, X. Li, C. Wang, *Chem. Commun.* **2011**, *47*, 3906–3998; c) A. Gangula, R. Podila, M. Ramakrishna, L. Karanam, C. Janardhana, A. M. Rao, *Langmuir* **2011**, *27*, 15268–15274; d) C. Wang, R. Ciganda, L. Yate, S. Moya, L. Salmon, J. Ruiz, D. Astruc, *J. Mater. Sci.* **2017**, *52*, 9465–9476.
- [24] S. Harish, J. Mathiyarasu, K. L. N. Phani, V. Yegnamaran, *Catal. Lett.* **2009**, *128*, 197–202.
- [25] B. Liu, S. Yu, Q. Wang, W. Hu, P. Jing, Y. Liu, W. Jia, Y. Liu, L. Liu, J. Zhang, *Chem. Commun.* **2013**, *49*, 3757–3759.
- [26] C. Deraedt, L. Salmon, D. Astruc, *Adv. Synth. Catal.* **2014**, *356*, 2525–2538.
- [27] H. Li, L. Han, J. Cooper-White, I. Kim, *Green Chem.* **2012**, *14*, 586–591.
- [28] K. Jiang, H. X. Zhang, Y. Y. Yang, R. Mothes, H. Lang, W. B. Cai, *Chem. Commun.* **2011**, *47*, 11924–11926.
- [29] X. Lu, X. Bian, G. Nie, C. Zhang, C. Wang, Y. Wei, *J. Mater. Chem.* **2012**, *22*, 12723–12730.
- [30] J. Morère, M. J. Tenorio, M. J. Torralvo, C. Pando, J. A. R. Renuncio, A. Cabanas, *J. Supercrit. Fluids* **2011**, *56*, 213–222.
- [31] R. Bhandari, M. R. Knecht, *ACS Catal.* **2011**, *1*, 89–98.
- [32] Y. Mei, G. Sharma, Y. Lu, M. Ballauff, M. Dreshler, T. Irrgang, R. Kempe, *Langmuir* **2005**, *21*, 12229–1234.
- [33] S. Gatard, L. Salmon, C. Deraedt, J. Ruiz, D. Astruc, S. Bouquillon, *Eur. J. Inorg. Chem.* **2014**, 4369–4375.
- [34] C. Wang, R. Ciganda, L. Salmon, D. Gregurec, J. Irigoyen, S. Moya, J. Ruiz, D. Astruc, *Angew. Chem. Int. Ed.* **2016**, *55*, 3091–3095; *Angew. Chem.* **2016**, *128*, 3143–3147.
- [35] F. Fu, A. M. Martínez-Villacorta, A. Escobar, J. Irigoyen, S. Moya, E. Fouquet, J. Ruiz, D. Astruc, *Inorg. Chem. Front.* **2017**, *4*, 2037–2044.
- [36] H. Yamamoto, H. Yano, H. Kouchi, Y. Obara, R. Arakawa, H. N. Kawasaki, *Nanoscale* **2012**, *4*, 4148–4154.
- [37] R. Fenger, E. Fertitta, H. Kirmse, A. F. Thunemann, K. Rademann, *Phys. Chem. Chem. Phys.* **2012**, *14*, 9343–9349.
- [38] E. Seo, J. Kim, Y. Hong, Y. S. Kim, D. Lee, B. S. Kim, *J. Phys. Chem. C* **2013**, *117*, 11686–11693.
- [39] C. Xiao, S. Chen, L. Zhang, S. Zhou, W. Wu, *Chem. Commun.* **2012**, *48*, 11751–11753.
- [40] T. Huang, F. Meng, L. Qi, *J. Phys. Chem. C* **2009**, *113*, 13636–13642.
- [41] J. Han, L. Li, R. Guo, *Macromolecules* **2010**, *43*, 10636–10644.
- [42] I. Biondi, G. Laurency, P. J. Dyson, *Inorg. Chem.* **2011**, *50*, 8038–8045.
- [43] K. Esumi, K. Miyamoto, T. Yoshimura, *J. Colloid Interface Sci.* **2003**, *268*, 501–506.
- [44] K. Hayakawa, T. Yoshimura, K. Esumi, *Langmuir* **2003**, *19*, 5517–5521.
- [45] N. Li, P. Zhao, N. Liu, M. Echeverría, S. Moya, L. Salmon, J. Ruiz, D. Astruc, *Chem. Eur. J.* **2014**, *20*, 8363–8369.
- [46] N. Li, M. Echeverría, S. Moya, J. Ruiz, D. Astruc, *Inorg. Chem.* **2014**, *53*, 11802–11808.
- [47] R. Ciganda, N. Li, C. Deraedt, S. Gatard, P. Zhao, L. Salmon, R. Hernandez, J. Ruiz, D. Astruc, *Chem. Commun.* **2014**, *50*, 10126–10129.
- [48] S. Das, B. G. Bag, R. Basu, *Appl. Nanosci.* **2015**, *5*, 867–873.
- [49] A. G. Majouga, E. K. Beloglazkina, E. A. Manzheliy, D. A. Denisov, E. G. Evtushenko, K. I. Maslakov, E. V. Golubina, N. V. Zyk, *Appl. Surf. Sci.* **2015**, *325*, 73–78.
- [50] Y. Ju, X. Li, J. Feng, Y. Ma, J. Hu, X. Chen, *Appl. Surf. Sci.* **2014**, *316*, 132–140.
- [51] H. Woo, J. W. Kim, M. Kim, S. Park, K. H. Park, *RSC Adv.* **2015**, *5*, 7554–7558.
- [52] P. Zhao, N. Li, N. Liu, L. Salmon, J. Ruiz, D. Astruc, *Chem. Commun.* **2013**, *49*, 3218–3220.
- [53] a) C. Deraedt, L. Salmon, L. Etienne, J. Ruiz, D. Astruc, *Chem. Commun.* **2013**, *49*, 8169–8171; b) C. Deraedt, D. Astruc, *Acc. Chem. Res.* **2014**, *47*, 494–503; c) S. Handa, Y. Wang, F. Gallou, B. H. Lipshutz, *Science* **2015**, *349*, 1087–1091.

Manuscript received: January 27, 2018

Accepted manuscript online: February 28, 2018

Version of record online: April 14, 2018